IEEE Access
Multidisciplinary ⋮ Rapid Review ⋮ Open Access Journal

Received 28 April 2024, accepted 15 May 2024, date of publication 21 May 2024, date of current version 30 May 2024.

Digital Object Identifier 10.1109/ACCESS.2024.3403666

STANDARDS

A Micro Radial-Torsional Vibration Ultrasonic Motor Driven by Single-Phase Signal

XIULI ZHENG[1], LE WANG[2,3], JUNMING LIU[4], AND SI CHEN[4]

[1]College of Optoelectronic Manufacturing, Zhejiang Industry and Trade Vocational College, Wenzhou 325003, China
[2]School of Intelligent Manufacturing and Elevator, Huzhou Vocational and Technical College, Huzhou 313099, China
[3]School of Mechanical Engineering, Guizhou University, Guiyang 550025, China
[4]College of Mechanical and Electrical Engineering, Wenzhou University, Wenzhou 325035, China

Corresponding author: Le Wang (20200315@wzu.edu.cn)

This work was supported in part by Zhejiang Provincial Natural Science Foundation of China under Grant LGG20E050003, in part by the Special Exploration Project for High-Level Talents of Huzhou Vocational and Technical College under Grant 2023TS06, in part by the General Scientific Research Projects of Zhejiang Provincial Department of Education under Grant Y202352861, and in part by the Natural Science Foundation of Jiangsu Higher Education Institutions of China under Grant 22KJB460003.

ABSTRACT Traditional mode conversion ultrasonic motors are typically composed of the superposition of multiple vibration modes, making them more complex than single-mode ultrasonic motors. This complexity makes it difficult to miniaturize. A micro radial-torsional vibration mode ultrasonic motor is proposed and tested in this work. It is excited by a single-phase excitation signal. The proposed motor utilizes the radial in-plane vibration mode of the stator to convert the torsional vibration mode of the inner ring through the beams. The torsional vibration of the inner ring causes the rotor to rotate due to the friction force between the inner ring and the rotor. Based on the designed structure and verified using the finite element method, a prototype motor with a mass of 2.6 g and overall dimensions of Ô20 mm in diameter and 15 mm in height is fabricated and characterized. During the mechanical output performance test, the prototype achieved a maximum no-load speed of 3300 r/min and a stall torque of 0.2 mN·m at the driving voltage of 100 V_{p-p}.

INDEX TERMS Ultrasonic motor, piezoelectric actuator, radial-torsional vibration, mode conversion.

I. INTRODUCTION

The continuous development of precision control technology puts forward higher requirements for the operating characteristics and environmental adaptability of the motor, which is particularly prominent in space satellite exploration and high-pressure deep sea [1], [2], [3]. The deficiencies of traditional electromagnetic motors, such as complex shape, high energy consumption and easy to be influenced by environmental factors have gradually restricted their application [4]. Therefore, researches on lightweight and high energy density motors suitable for vacuum space with low temperature and strong pressure has always been a hot spot. As a new type of friction drive motor, ultrasonic motor has compact structure, rapid response and no electromagnetic interference when working [5], [6], [7]. These merits meet the needs of stable and reliable operation under complex and harsh working conditions, and have become a focus of attention in recent years.

Generally speaking, different electrical signals are applied to two groups of piezoelectric ceramics in the ultrasonic motor to excite the corresponding vibration modes of the stator drive. Then the traveling waves on the stator driving interface or elliptical trajectories of particles on its surface are formed through the coupling of these vibration modes, thus promoting the rotation of rotor. Traditional traveling-wave rotary ultrasonic motors (TRUMS) [8], [9], [10], [11], [12], longitudinal torsional composite ultrasonic motors (LTUMS) [13], [14], V-shaped linear ultrasonic motors [15], [16] and disk ultrasonic motors are coupled by two vibration modes and driven by two-phase electrical signals. Although their output torques are large, the standards of structural design, piezoelectric ceramic performance and driving controller are high. In contrast, the control of single-mode motor driven by single-phase excitation signal is simpler, which is more suitable for underwater working environment and

The associate editor coordinating the review of this manuscript and approving it for publication was Michail Kiziroglou.

miniaturization of robot. According to the driving principle, single-mode ultrasonic motors can be roughly divided into inertial ultrasonic motors [17], [18], [19], standing wave ultrasonic motors [20], [21] and mode conversion motors [22], [23]. Modal conversion ultrasonic motors mostly adopt columnar sandwich structure, and the longitudinal vibration mode of the stator is converted to torsional vibration mode by opening inclined slots on the stator. Based on this method, J. Tsujino et al. proposed a longitudinal-torsional mode conversion rotary ultrasonic motor [22]. Palmer and others use this kind of motor as the driving mechanism of micro robot [23]. The utilize of sandwich structure is helpful to improve torque, but its application space is limited to some extent by the strict machining accuracy and large stator height. For miniature ultrasonic motors, a simple structure will drastically reduce the difficulty and cost of machining, and a series of products can be formed, such as the series of submillimeter miniature ultrasonic motors proposed by Kikuchi et al. [24], [25], [26], [27]. Therefore, further study on the compact ultrasonic motor with modal conversion is still of great practical significance.

This work proposes a radial-torsional vibration modal ultrasonic motor with a patch structure. Firstly, the structure of the ultrasonic motor operating in radial-torsional vibration mode is designed, and its sequential operational processes are analyzed. Next, finite element methods are utilized to calculate the vibration modes and the corresponding resonance frequency of the motor. Finally, a prototype motor has been manufactured and tested. The optimal driving waveform and the mechanical output performance of the motor are being discussed.

II. OPERATING PRINCIPLE OF THE MOTOR

A. STRUCTURE DESIGN

As shown in Figure 1(a), the proposed motor is mainly composed of a clamping, a spring, rotor 1, a substrate, an annular piezoelectric wafer and a shaft rotor 2. The shaft and rotor are fixed on the upper and lower driving surfaces of the inner ring through the spring and nut. The spring contributes to the adjustment of pre-pressure between the rotor and stator. The inner ring is connected with the outer ring through connecting beams tangent to its outer side. One piece of piezoelectric wafer is pasted on the bottom surface of the outer ring of the stator to excite the in-plane vibration mode of the stator. Considering the difficulty and cost of machining in the design stage of the prototype, the design of fixed position of the motor with other mechanical structures was cancelled. Similar micro motors without fixed positions can be seen in the micro motor series designed by T. Mashimo [24], [25], [26], [27]. The main dimensions of the stator are given in Figure 1(b)and Table 1.

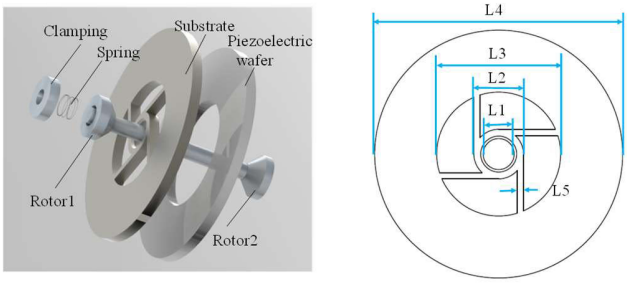

FIGURE 1. Construction of the proposed motor structure: (1) components of the motor; (2) main dimensions of the stator.

TABLE 1. The main dimensions of the stator (unit: MM).

Parameter	L1	L2	L3	L4	L5
Value	2.5	4	10	20	0.5

B. OPERATING PRINCIPLE

When an excitation signal is applied to the piezoelectric wafer, it can excite the radial expansion vibration mode of the stator's outer ring. The connecting beam can transform the radial expansion vibration mode of the stator's outer ring into the torsional vibration mode of the inner ring. This excites the particles on the inclined driving interface of the inner ring, generating linear motion in the tangential direction and driving the rotor's rotation through friction between the stator and the rotor. Figure. 2 illustrates the movement process of the motor during a single working cycle, which consists of four stages.

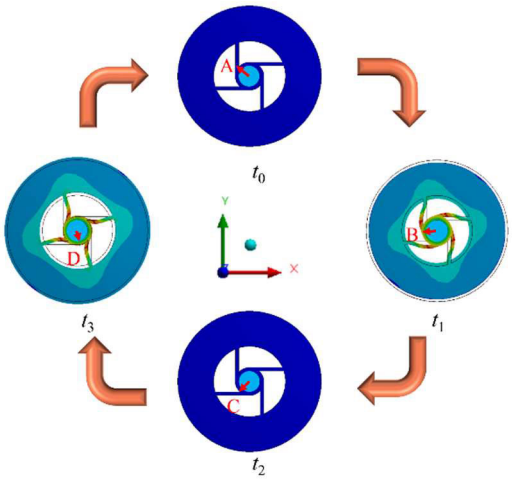

FIGURE 2. Operating principle of the motor.

Stage I: When the outer ring of the stator contracts radially, the inner ring twists in a counterclockwise direction. Under the influence of friction, the rotor accelerates from the initial position A to position B during t0 ∼ t1.

Stage II: During t1 ∼ t2, the recovery deformation of the outer ring leads to the reverse torsion recovery of the inner ring. The rotor decelerates, but due to sliding friction, it continues to rotate and changes from position B to position C.

Stage III: When the outer ring expands rapidly along the radial direction, the inner ring twists in the opposite direction from its initial state. The rotor continues to decelerate as it moves from position C to position D during t2 ∼ t3 is due to the inertial force.

Stage IV: When the outer ring and inner ring are restored to their original positions in t3 ∼ t0, the rotor is accelerated again under the action of friction.

By repeating the four successive steps described above, the stator can drive the rotor through friction to sustain a counterclockwise rotation. Nevertheless, due to the asymmetrical design of the connecting beam in the stator structure, the proposed motor only allows for unidirectional rotation.

III. FINITE ELEMENT MODELING AND SIMULATION OF STATOR

As shown in Figure 3(a), a finite element model (FEM) of the stator was built by the finite element software ANSYS. The polarization direction of the piezoelectric ceramic plate is defined in the established base vector coordinate system, and a 10 V_{p-p} AC electric signal is applied to it. The model has a free boundary mechanical boundary condition, and its main material parameters are listed in Table 2. The mesh accuracy of the finite element model of the motor stator is set to normal. It is automatically divided into 3699 titanium alloy matrix elements and 1302 PZT-8 piezoelectric ceramic elements by the software based on the physical field. In the process of solving, the damping loss coefficients of titanium alloy and PZT-8 piezoelectric ceramics are set to 0.005 and 0.01, respectively [28]. The first-order radial expansion vibration mode (see Figure 3(b)) of the stator is obtained through modal calculation. In this working mode, the stator's corresponding characteristic frequency is 89.518 kHz. At this time, the outer ring periodically expands radially, and the inner ring rotates accordingly. This vibration mode proves the feasibility of the motor's working principle.

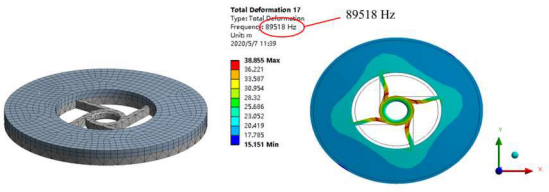

FIGURE 3. Finite element simulation of motor stator: (a) three-dimensional model; (b) operating mode of stator.

The dynamic characteristics of the ultrasonic motor stator directly impact the motor's output performance. Therefore, it is essential to conduct further analysis of the dynamic characteristics of particles on the driving surface of the stator. A unit particle P is selected, and its position on the driving surface of the stator is marked in Figure 4(a). The corresponding movement displacement of point P under 10 V_{p-p} excitation

TABLE 2. Major material characteristic parameters of stator model.

Materials	PZT-8	Titanium alloy
Density (kg/m3)	7650	450
Poisson's ratio	0.31	0.34
Elastic modulus ($\times 1010 N/m^2$)	$\begin{bmatrix} 12.06 & 5.35 & 5.15 & 0 & 0 & 0 \\ 5.35 & 12.06 & 5.15 & 0 & 0 & 0 \\ 5.15 & 5.15 & 10.45 & 0 & 0 & 0 \\ & & & 3.13 & 0 & 0 \\ & & & & 3.13 & 0 \\ & & & & & 3.46 \end{bmatrix}$	110
Piezoelectric constant (C/m^2)	$\begin{bmatrix} 0 & 0 & -5.2 \\ 0 & 0 & -5.2 \\ 0 & 0 & 15.1 \\ 0 & 0 & 0 \\ 0 & 12.7 & 0 \\ 12.7 & 0 & 0 \end{bmatrix}$	-

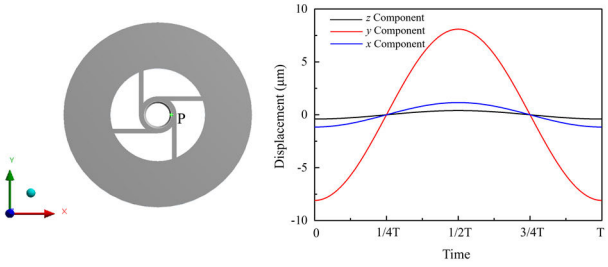

FIGURE 4. Calculation of motion displacement of driving point P on the driving plane: (a) position of point P; (b) displacements of point P in different directions during a working period.

voltage can be obtained through harmonic response analysis and calculation, as shown in Figure 4(b). By analyzing the displacement amplitude parameters, it can be observed that the displacement of point P in the Y-axis direction is significantly greater than that in the X-axis and Z-axis directions. Associated with the position of point P, it is evident that the displacement of particles on the driving surface in this mode mainly occurs in the tangent direction of this point. The displacement in the Z-axis direction is nearly zero, indicating that the structure's vibration mode is primarily radial in the plane at an excitation frequency of 89.518 kHz.

Moreover, analyzing the trajectory of point P helps to enhance understanding of the motor's operation. The trajectory depicted in Figure 5 appears as an inclined straight line, which conforms to the friction driving principle of ultrasonic motor. The finite element analysis confirms that the motor stator's working mode can effectively drive the rotor to rotate through friction, meeting the necessary requirements.

Based on the above analysis, the key components and dimensions of the motor have been optimized. Firstly, the number of beams connecting the inner and outer rings is optimized. The performance of the motor is determined by the magnitude of the total displacement of the stator. The relationship between the total stator displacement and the

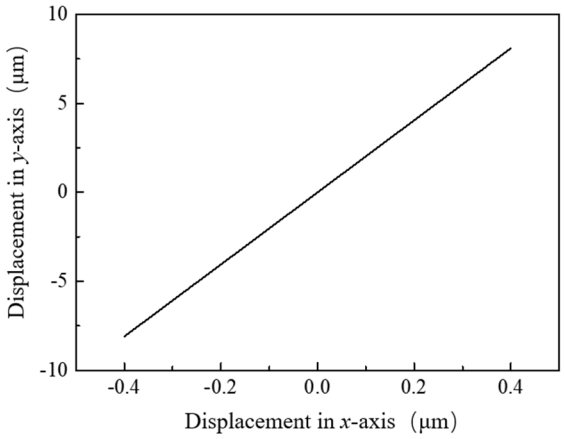

FIGURE 5. Trajectory of driving point P in the XOY plane.

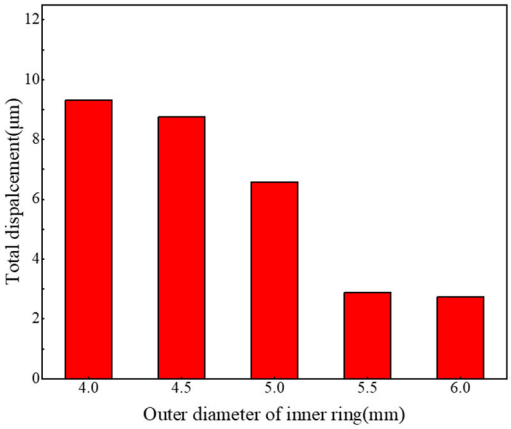

FIGURE 7. The relationship between the total displacement and the outer diameter of the inner ring.

number of beams can be obtained from the harmonic response analysis as shown in Figure 6. From the harmonic response analysis results, it can be seen that the total displacement is maximum when the number of beams is 4. Therefore, the number of connected beams is set to 4. Then the outer diameter of the inner ring was also optimized. The range of changing the outer diameter size of the inner ring is set to 4 mm to 6 mm, and the step size is set to 0.5 mm, and then the harmonic response analysis is carried out, and the structure of the analysis is shown in Figure 7. From the analysis results, it can be seen that the total displacement decreases as the outer diameter size increases, so the outer diameter size is set to 4mm.

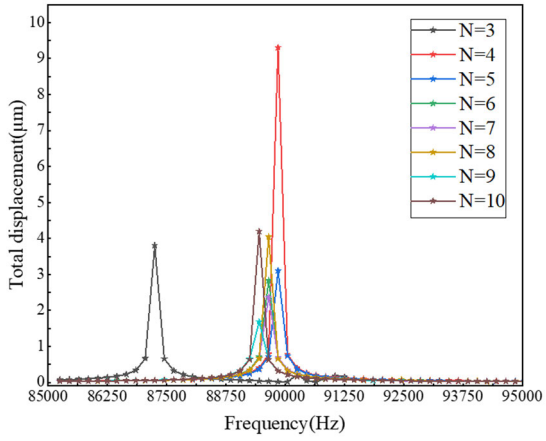

FIGURE 6. The relationship between the total displacement and the number of connecting beams under the same mode.

IV. EXPERIMENT AND RESULT ANALYSIS

Based on the motor structure design and an analysis of its working principle, a prototype of an ultrasonic motor is fabricated and assembled. The prototype has a total mass of approximately 2.6 grams and the overall size is 20 mm in diameter and 15 mm in height as shown in Figure 8.

Use epoxy resin to adhere functional piezoelectric ceramic sheets (PZT-8, Sinocera Piezotronics. Inc, China) to the surface of the stator. Except for the stainless-steel spring, all other parts of the motor are made of titanium alloy, and the stator matrix is created using a wire-cutting process. The prototype is used as the experimental subject, and the mechanical vibration characteristics of the motor are tested subsequently.

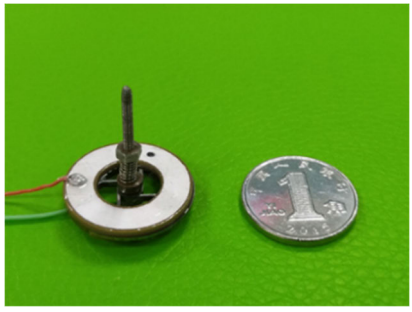

FIGURE 8. Prototype of the proposed motor.

A three-dimensional Doppler laser vibrometer (PSV-500-3D, Polytec GmbH, Waldbronn, Germany) is employed to analyze the vibration characteristics of the stator surface of the motor. Figure 9 shows the amplitude-frequency response curve of the stator, which was generated by applying a driving voltage of 10 V_{p-p} to the stator ceramics. The characteristic frequency of the first-order radial vibration mode of the stator is 89.687 kHz, which is largely consistent with the theoretical value. However, there is a slight discrepancy of 89.518 kHz ($< 0.2\%$). The reasons for the difference are related to the clamping of the stator during experimental testing, while the boundary conditions in finite element simulation are free states. In addition, Neglecting the adhesive layer between the stator and PZT in finite element analysis is also one of the reasons for the difference in resonant frequency. The local vibration mode of the stator is then tested

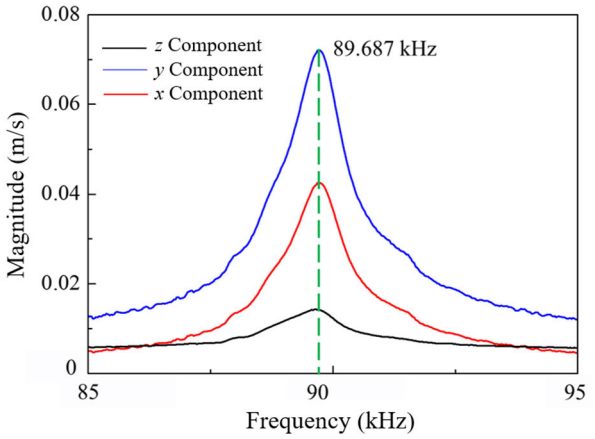

FIGURE 9. Frequency sweeping test results.

at a vibration frequency of 89.687 kHz, as shown in Figure 10. The modal shapes of the stator's outer ring (Figure 10(a)), the inner ring (Figure 10(b)), and the connecting beams (Figure 10(c)) correspond to those obtained from the finite element method simulation. This further validates the rationality of the motor's structural design and the accuracy of the simulation calculations.

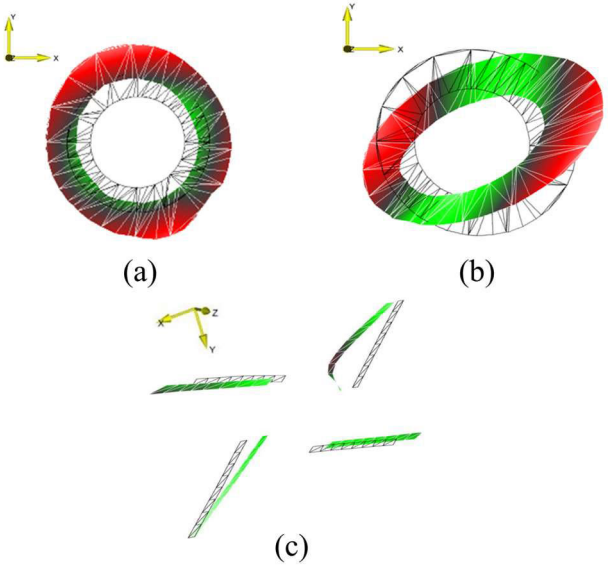

FIGURE 10. Test results of stator mode shapes. (a) Vibration shape of the outer ring. (b) Vibration shape of the inner ring. (c) Vibration shape of the beams.

The electrical characteristics of the stator are another important index for evaluation. An impedance analyzer (PSV80A, Beijing Liangang Times Technology Co., Ltd.) is used for testing. The test frequency ranges from 85 kHz to 95 kHz, and the built-in voltage of the impedance analyzer is set to 0.5 V_{p-p}, eliminating the need to apply additional electrical signals to the stator. In the admittance diagram shown in Figure 11(a), the admittance circle is nearly a complete circle. This pattern indicates that the piezoelectric device is an undamaged acoustic structure. The resonance frequency of the stator is 89.924 kHz, as indicated in the impedance-frequency characteristic curve of the stator in Figure 11(b). This value closely aligns with both the simulation calculation and the results of the mechanical vibration test, with only a slight difference. The main reasons for this deviation are the motor's clamping mode and the system test error. Meanwhile, the quality parameter QM of 387.438 can be obtained through impedance analysis.

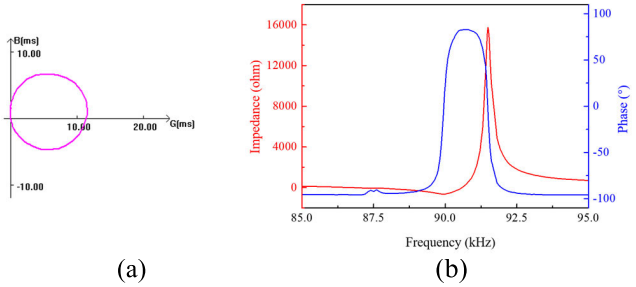

FIGURE 11. Admittance and impedance characteristics of stator frequency: (a) The stator admittance circle diagram; (b) The stator impedance characteristic of the stator.

To accurately control the motor, it is necessary to analyze the relationship between the rotational speed and frequency of the prototype using experimental methods. Here, the motor speed testing device shown in Figure 12 is set up. The laser velocimeter (DT6234C, Shenzhen Yusheng Electronic Technology Co.) is utilized for measuring the motor's speed. The method of the test is shown in Figure 12. The input voltage is a 100 V_{p-p} square wave signal, and the preload pressure is adjusted to 0.3 N. Figure 13 illustrates the experimental results of prototype rotary speeds at various frequencies. From Figure 14, the rotation speed of the prototype initially increases and then decreases as the frequency rises. The maximum rotation speed shows at 89.8 kHz, which is considered the optimal driving frequency. The rotation speed of the motor has been tested in relation to the voltage at different preload and the results are shown in Figure 14. From the results it can be seen that the rotation speed of the motor is positively correlated with the increase in voltage. As the preload increases, the speed of the motor decreases in a negative correlation. Therefore, the preload force was set to 0.3 N in order to obtain a higher speed.

On the other hand, the waveform of the electrical signal will also affect the output performance of the motor. The sine wave signal, square wave signal, and sawtooth wave signal are selected and applied to the prototype to study their influence on the motor's output performance. The preload between the stator and rotor of the motor prototype is set to 0.3 N, and the driving frequency is set to 89.8 kHz. Figure 15 illustrates the relationship between motor speed and voltage driven by three different waveform signals. It is evident that regardless of the signal being applied, the speed of the prototype motor exhibits a linear growth trend with

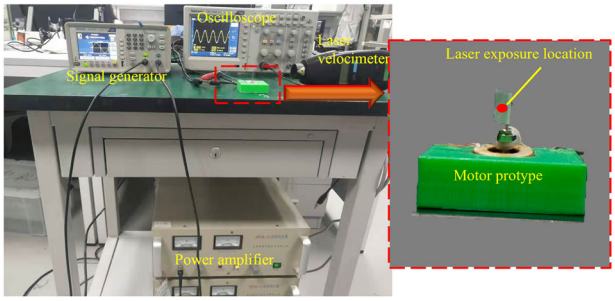

FIGURE 12. Layout of motor rotating speed test device.

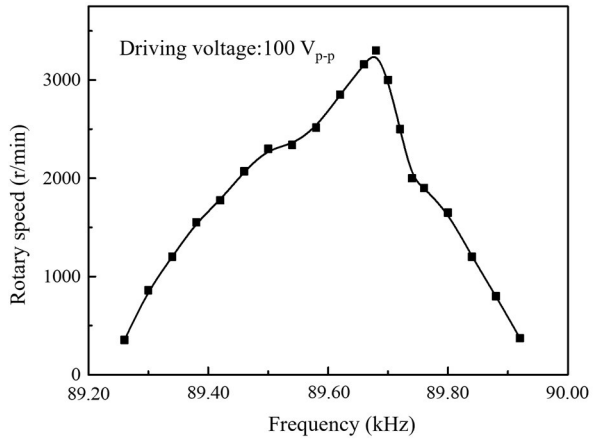

FIGURE 13. Rotary speed of the prototype versus driving frequency.

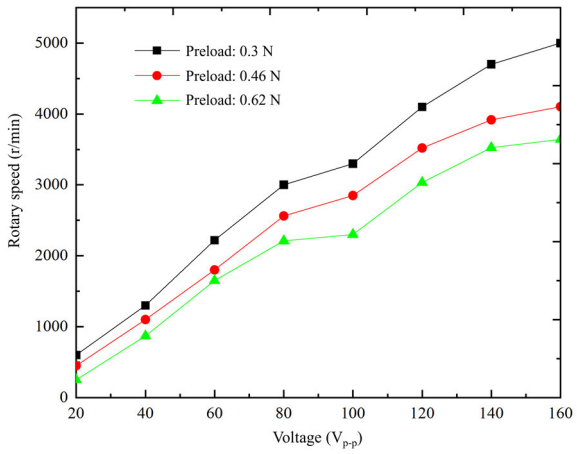

FIGURE 14. The relationship between speed and voltage under different preload.

increasing voltage. This phenomenon demonstrates that all three signals can effectively drive the motor. Moreover, the motor driven by a square wave signal achieves a higher speed at the same excitation voltage compared to the other two types. It reaches a maximum value of 5000 r/min at 160 V_{p-p}. In light of this, the square wave signal is more suitable for this type of motor drive.

To deeply explore the causes of this phenomenon, the vibration velocity waveforms are analyzed in detail.

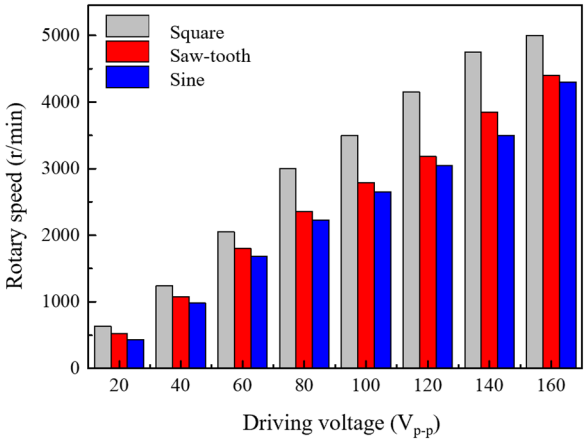

FIGURE 15. Rotational speed versus voltage for motors with different drive signals.

A three-dimensional Doppler laser vibrometer was utilized to test the vibration velocity waveforms of a unit particle on the interface of the motor's inner ring, which was actuated by different input signals. The test results are respectively shown in Figures 16(a) ∼ (c). As shown in Figures 16 (a) to (c), the observed vibration velocity waveforms of particles along the x-axis and y-axis correspond to different driving signals, all of which are sine wave shapes. The amplitudes shown in Figure 16(a) and Figure 16(b) are close to that in Figure 16(c) because the driving frequency is close to the resonance frequency of radial vibration in the plane [20], [29], [30]. However, the vibration velocity waveforms in the z-axis direction are different. According to the relationship between velocity and displacement, it can be concluded that the displacement waveform in the z-axis direction. The amplitude of the displacement in the z-axis direction is much smaller than the displacements in the other two directions in both the finite element analysis and the vibration measurement experiments (see Figure 4 and Figure 16), which is almost an order of magnitude smaller. The experimental results prove that under different drive signals, the vibration waveforms in the z-axis direction are different, and it is this difference that leads to the difference in the performance of the motors. When the input signal is set as a sawtooth wave, the vibration velocity waveform of the same particle on the driving interface along the x-axis and y-axis is a sine wave, and the vibration velocity waveform along the z-axis is also a sawtooth wave (see Figure 16(c)). The asymmetric displacement signal in the z-axis direction results in less speed attenuation of the motor during the deceleration stage, thus improving the motor's performance. This phenomenon can be explained by the driving principle of piezoelectric inertial motors. This experiment also shows that the performance of standing wave ultrasonic motors driven by square-wave signals is better than that of sinusoidal drive signals. However, the micro-amplitude vibration in the z-axis direction is not sufficient to affect the operating principle of the motor, but only contributes to the performance of the motor.

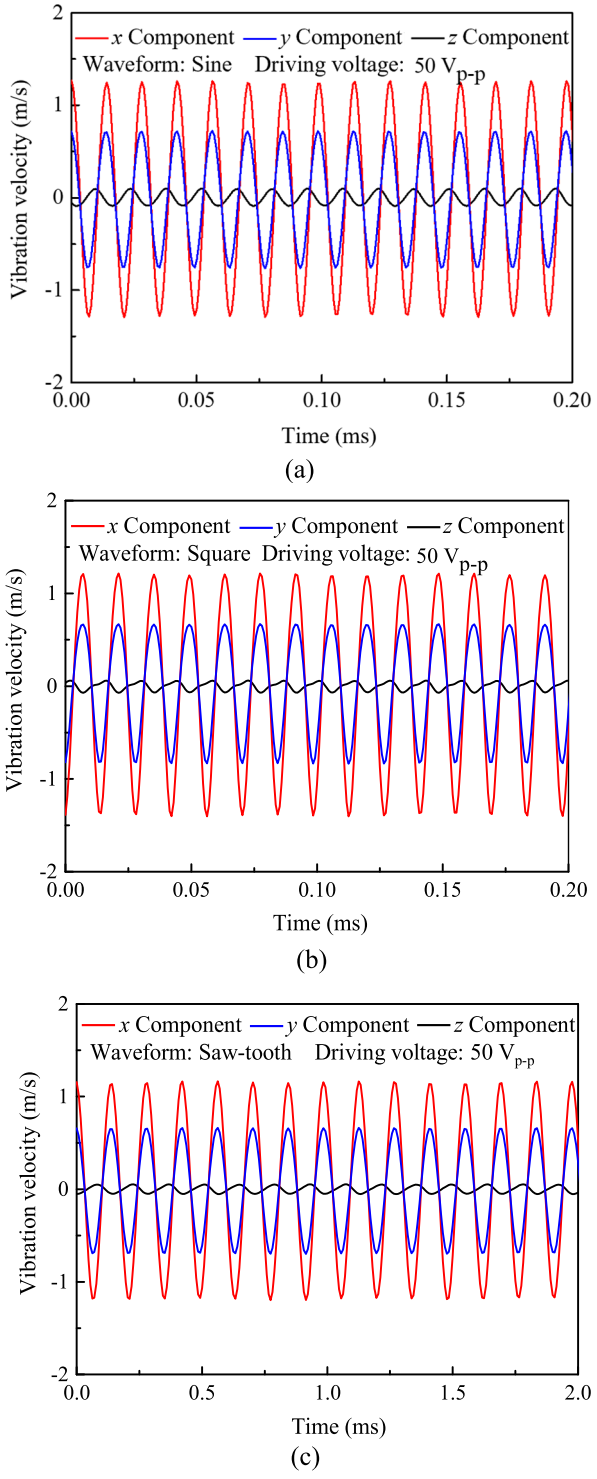

FIGURE 16. (a) Vibration velocity with a sin wave signal; (b) vibration velocity with a square wave signal; (b) vibration velocity with a saw-tooth wave signal.

Therefore, when using a square wave signal or a sawtooth wave to drive the motor. This law is similar to that of inertial ultrasonic motors [19], [29], [30], [31].

On account of the experiments above, the optimal driving frequency of the motor is established as 89.8 kHz. Then the pre-pressure between the stator and rotor is adjusted to 0.3 N, and the driving voltage is set to 100 V_{p-p}. On these premises the mechanical output performance of the prototype is experiment-studied at room temperature. Figure 17 signifies that the maximum no-load speed of the prototype is 3300 r/min and the stall torque is 0.20 mN · m. As inferred from the experimental results, when the load of the prototype is 0.08 mN · m, the maximum output power can reach 0.019 W. The above basic experiments indicate that the proposed motor has good mechanical output performance, and combined with the waterproof characteristics of ultrasonic motors, it is expected to be used for driving micro underwater robots.

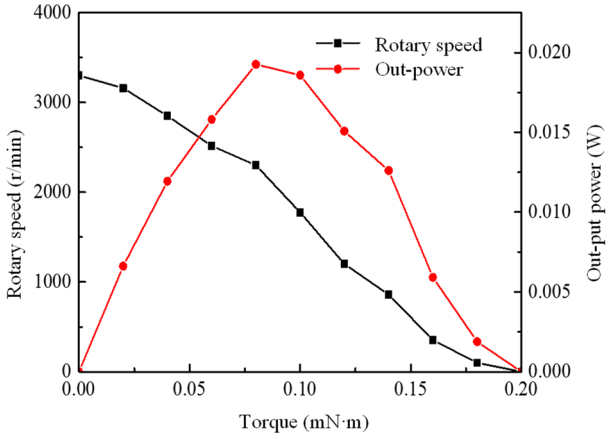

FIGURE 17. Mechanical characteristic curve of the motor prototype.

The performance of the proposed motor is compared with several previous single-phase ultrasonic motors and disk shape ultrasonic motors, as listed in Table 3. Qiu et al. proposed a disc type piezoelectric motor with a maximum no-load speed of 5172 rpm. This is a good structural design, and the thin stator design results in a very low drive voltage, reducing the requirement for a drive controller [32]. He et al. proposed two standing wave motors with different configurations, which require only a single-phase excitation signal to drive, with speeds of 400 rpm and 1000 rpm, respectively [21], [33]. Pan introduced an ultrasonic motor with an asymmetric stator and four drive legs. The motor has a no-load speed of 176.5 rpm and a maximum torque of 29.4 mN·m [20]. A compact symmetric coplanar piezoelectric motor for high-speed rotary motors up to 5000 rpm was presented by Pan et al. [34]. Compared with these motors, the speed of the motor proposed in this paper can reach their highest level. In addition, the biggest advantage of the motor in this paper is the expandability of the structure, which can be derived from a series of motors with the same structure and different sizes. Moreover, the processing difficulty and cost are greatly reduced, and laser processing can be used for processing, which makes the processing efficiency higher, and this point has been verified in the latest work.

TABLE 3. Features of single-phase ultrasonic motors.

	Top rotary speed(r/min)	Top torque(mN·m)
Qiu et al [32]	5172	0.35
He et al [33]	400	0.3
He et al [21]	1000	0.37
Pan et al [20]	176.5	29.4
Borodinas et al [35]	5000	/
This work	5000	0.20

V. CONCLUSION

A micro mode conversion ultrasonic motor using radial-torsional vibration mode was proposed. Based on the FEM modal analysis, a prototype motor was manufactured and relevant mechanical and electrical characteristic tests were carried out to obtain the optimal driving frequency and waveform. Major mechanical characteristics of the prototype motor include the maximum speed of 3300 r/min, maximum stall torque of 0.20 mN·m, and maximum output power of around 0.019 W. The advantage of the proposed modal-conversion motor is that its structure is much simpler than that of traditional modal-conversion motors, which drastically reduces the processing difficulty and cost, and it can be derived from a series of products with different sizes.

CONFLICT OF INTEREST STATEMENT

The author declares that the research was conducted in the absence of every commercial or financial relationships that could be construed as a potential conflict of interest.

REFERENCES

[1] S. He, S. Shi, Y. Zhang, and W. Chen, "Design and experimental research on a deep-sea resonant linear ultrasonic motor," *IEEE Access*, vol. 6, pp. 57249–57256, 2018.
[2] J. Liu, Z.-J. Niu, H. Zhu, and C.-S. Zhao, "Design and experiment of a large-aperture hollow traveling wave ultrasonic motor with low speed and high torque," *Appl. Sci.*, vol. 9, no. 19, p. 3979, Sep. 2019.
[3] S. He, S. Shi, and W. Chen, "Development of deep-sea resonant sandwich linear ultrasonic motor," *J. Appl. Math. Phys.*, vol. 6, no. 1, pp. 296–300, 2018.
[4] X. Lu, Z. Wang, H. Shen, K. Zhao, T. Pan, D. Kong, and J. Twiefel, "A novel dual-rotor ultrasonic motor for underwater propulsion," *Appl. Sci.*, vol. 10, no. 1, p. 31, Dec. 2019.
[5] X. DongMei, Z. BingJie, Y. SiMiao, and Z. XuHui, "Review on single-phase driven ultrasonic motors," *J. Intell. Mater. Syst. Struct.*, vol. 34, no. 5, pp. 525–535, Mar. 2023.
[6] D. An, M. Yang, X. Zhuang, T. Yang, F. Meng, and Z. Dong, "Dual traveling wave rotary ultrasonic motor with single active vibrator," *Appl. Phys. Lett.*, vol. 110, no. 14, Apr. 2017, Art. no. 143507.
[7] J. Yan, Y. Liu, J. Liu, D. Xu, and W. Chen, "The design and experiment of a novel ultrasonic motor based on the combination of bending modes," *Ultrasonics*, vol. 71, pp. 205–210, Sep. 2016.
[8] R. Q. Rudy, G. L. Smith, D. L. DeVoe, and R. G. Polcawich, "Millimeter-scale traveling wave rotary ultrasonic motors," *J. Microelectromech. Syst.*, vol. 24, no. 1, pp. 108–114, Feb. 2015.
[9] A. Iula and M. Pappalardo, "A high-power traveling wave ultrasonic motor," *IEEE Trans. Ultrason., Ferroelectr., Freq. Control*, vol. 53, no. 7, pp. 1344–1351, Jul. 2006.
[10] W. Chen, S. Shi, Y. Liu, and P. Li, "A new traveling wave ultrasonic motor using thick ring stator with nested PZT excitation," *IEEE Trans. Ultrason., Ferroelectr., Freq. Control*, vol. 57, no. 5, pp. 1160–1168, May 2010.
[11] X. Li, T. Huang, N. Zhao, Y. Shen, J. Huang, X. Li, J. Li, and L. Yang, "A design method of traveling wave rotary ultrasonic motors driving circuit under high voltage using single-sided Hertzian contact forced oscillator model," *Micromachines*, vol. 14, no. 1, p. 64, Dec. 2022.
[12] D. Lu, H. Liu, J. Xu, T. Yang, and H. Hu, "A linear ultrasonic motor based on coupling vibration mode," *Micromachines*, vol. 13, no. 11, p. 1852, Oct. 2022.
[13] K. Nakamura, M. Kurosawa, and S. Ueha, "Characteristics of a hybrid transducer-type ultrasonic motor," *IEEE Trans. Ultrason., Ferroelectr., Freq. Control*, vol. 38, no. 3, pp. 188–193, May 1991.
[14] M. Kurosawa and S. Ueha, "Hybrid transducer type ultrasonic motor," *IEEE Trans. Ultrason., Ferroelectr., Freq. Control*, vol. 38, no. 2, pp. 89–92, Mar. 1991.
[15] K. Asumi, R. Fukunaga, T. Fujimura, and M. Kuribayashi Kurosawa, "High speed, high resolution ultrasonic linear motor using V-shape two bolt-clamped langevin-type transducers," *Acoust. Sci. Technol.*, vol. 30, no. 3, pp. 180–186, 2009.
[16] X. Li, Z. Yao, and M. Yang, "A novel large thrust-weight ratio V-shaped linear ultrasonic motor with a flexible joint," *Rev. Sci. Instrum.*, vol. 88, no. 6, Jun. 2017, Art. no. 065003.
[17] T. Morita, "Miniature piezoelectric motors," *Sens. Actuators A, Phys.*, vol. 103, no. 3, pp. 291–300, Feb. 2003.
[18] T. Morita, R. Yoshida, Y. Okamoto, M. K. Kurosawa, and T. Higuchi, "A smooth impact rotation motor using a multi-layered torsional piezoelectric actuator," *IEEE Trans. Ultrason., Ferroelectr., Freq. Control*, vol. 46, no. 6, pp. 1439–1445, Nov. 1999.
[19] T. Nishimura, H. Hosaka, and T. Morita, "Resonant-type smooth impact drive mechanism (SIDM) actuator using a bolt-clamped Langevin transducer," *Ultrasonics*, vol. 52, no. 1, pp. 75–80, Jan. 2012.
[20] S. Park and S. He, "Standing wave brass-PZT square tubular ultrasonic motor," *Ultrasonics*, vol. 52, no. 7, pp. 880–889, Sep. 2012.
[21] S. He, W. Chen, X. Tao, and Z. Chen, "Standing wave bi-directional linearly moving ultrasonic motor," *IEEE Trans. Ultrason., Ferroelectr., Freq. Control*, vol. 45, no. 5, pp. 1133–1139, Sep. 1998.
[22] J. Tsujino, M. Takeuchi, and H. Koshisako, "Ultrasonic rotary motor using a longitudinal-torsional vibration converter," in *Proc. IEEE Ultrason. Symp.*, Tucson, AZ, USA, 1992, pp. 887–892.
[23] H. Al-Budairi, P. Harkness, and M. Lucas, "A strategy for delivering high torsionality in longitudinal-torsional ultrasonic devices," *Appl. Mech. Mater.*, vol. 70, pp. 339–344, Aug. 2011.
[24] K. Kikuchi, M. Hussain, and T. Mashimo, "Fabrication and characterization of a submillimeter-scale ultrasonic motor," *Sens. Actuators A, Phys.*, vol. 360, Oct. 2023, Art. no. 114524.
[25] E. T. K. Chiang, T. Urakubo, and T. Mashimo, "Lift generation by a miniature piezoelectric ultrasonic motor-driven rotary-wing for pico air vehicles," *IEEE Access*, vol. 10, pp. 13210–13218, 2022.
[26] T. Mashimo and Y. Oba, "Performance improvement of micro-ultrasonic motors using the thickness shear mode piezoelectric elements," *Sens. Actuators A, Phys.*, vol. 335, Mar. 2022, Art. no. 113347.
[27] E. T. K. Chiang and T. Mashimo, "Comparison study of bending and three-wave vibration modes for micro ultrasonic motors," *Sens. Actuators A, Phys.*, vol. 329, Oct. 2021, Art. no. 112801.
[28] S. Borodinas, P. Vasiljev, and D. Mazeika, "The optimization of a symmetrical coplanar trimorph piezoelectric actuator," *Sens. Actuators A, Phys.*, vol. 200, pp. 133–137, Oct. 2013.
[29] T. Morita, T. Nishimura, R. Yoshida, and H. Hosaka, "Resonant-type smooth impact drive mechanism actuator operating at lower input voltages," *Jpn. J. Appl. Phys.*, vol. 52, no. 7S, Jul. 2013, Art. no. 07HE05.
[30] Y. Ma, H. Shekhani, X. Yan, M. Choi, and K. Uchino, "Resonant-type inertial impact motor with rectangular pulse drive," *Sens. Actuators A, Phys.*, vol. 248, pp. 29–37, Sep. 2016.
[31] M. Hunstig, T. Hemsel, and W. Sextro, "High-velocity operation of piezoelectric inertia motors: Experimental validation," *Arch. Appl. Mech.*, vol. 86, no. 10, pp. 1733–1741, Oct. 2016.
[32] J. Qiu, Y. Yang, X. Hong, P. Vasiljev, D. Mazeika, and S. Borodinas, "A disc-type high speed rotary ultrasonic motor with internal contact teeth," *Appl. Sci.*, vol. 11, no. 5, p. 2386, Mar. 2021.
[33] S. He, P. R. Chiarot, and S. Park, "A single vibration mode tubular piezoelectric ultrasonic motor," *IEEE Trans. Ultrason., Ferroelectr., Freq. Control*, vol. 58, no. 5, pp. 1049–1061, May 2011.

[34] Q. Pan, J. Hu, E. Miao, S. Chen, S. Shu, P. Hu, and B. Huang, "Novel piezoelectric rotary motor driven by a single-phase sine wave with an asymmetric stator," *Rev. Sci. Instrum.*, vol. 90, no. 7, Jul. 2019, Art. no. 075006.

XIULI ZHENG received the master's degree in mechanical engineering from Fuzhou University, China, in 2015. She is currently an Assistant Professor with the Optoelectronics Department, Zhejiang Industry and Trade Vocational College, China. She has also written dozens of books on the topic of industrial control and CNC machine tools. Her research interests include intelligent manufacturing and detection technology, especially in the domain of industrial robots, motors, and related material applications.

LE WANG was born in Shanxi, China. He received the Ph.D. degree from the College of Aerospace Engineering, Nanjing University of Aeronautics and Astronautics (NUAA), Nanjing, China, in 2020. From September 2020 to January 2023, he was a Lecturer with Wenzhou University. In January 2023, he transferred to work with Huzhou Vocational and Technical College. At the same time, he was a Postdoctoral Fellow with Guizhou University. His main research interests include novel ultrasonic motor design and bio-inspired flapping wing rotor design. He has published over 20 articles in these research interests.

JUNMING LIU received the B.S. degree in mechanical design, manufacturing and automation from Jiangsu University of Science and Technology, Zhenjiang, China, in 2021. He is currently pursuing the M.A.Eng. degree in mechanical and electrical engineering with Wenzhou University. His research interests include piezoelectric actuators and design of underwater microrobots.

SI CHEN was born in Zhenjiang, China, in 1993. He received the B.Eng. and Ph.D. degrees from Nanjing University of Aeronautics and Astronautics (NUAA), Nanjing, China, in 2015 and 2020, respectively. From 2016 to 2018, he went to the U.K. and studied at Cranfield University as a Joint Training Ph.D. Student. After graduating from NUAA, he was a Lecturer with Wenzhou University. His research interests include flapping wing and unsteady aerodynamic calculation. He has authored or coauthored ten internationally refereed articles in these research interests.